



HAL
open science

Hydrothermal fluid flow triggered by an earthquake in Iceland

Laurent Geoffroy, Catherine Dorbath, Kristján Ágústsson, Sigrídur Kristjánsdóttir, Ólafur G. Flóvenz, Cécile Doubre, Ólafur Gudmundsson, Thibaut Barreyre, Sarah Bazin, Aurore Franco

► **To cite this version:**

Laurent Geoffroy, Catherine Dorbath, Kristján Ágústsson, Sigrídur Kristjánsdóttir, Ólafur G. Flóvenz, et al.. Hydrothermal fluid flow triggered by an earthquake in Iceland. *Communications Earth & Environment*, 2022, 3, 10.1038/s43247-022-00382-0 . insu-03684621

HAL Id: insu-03684621

<https://insu.hal.science/insu-03684621>

Submitted on 1 Jun 2022

HAL is a multi-disciplinary open access archive for the deposit and dissemination of scientific research documents, whether they are published or not. The documents may come from teaching and research institutions in France or abroad, or from public or private research centers.

L'archive ouverte pluridisciplinaire **HAL**, est destinée au dépôt et à la diffusion de documents scientifiques de niveau recherche, publiés ou non, émanant des établissements d'enseignement et de recherche français ou étrangers, des laboratoires publics ou privés.



Distributed under a Creative Commons Attribution 4.0 International License

Hydrothermal fluid flow triggered by an earthquake in Iceland

Laurent Geoffroy ¹✉, Catherine Dorbath², Kristján Ágústsson³, Sigríður Kristjánsdóttir³, Ólafur G. Flóvenz³, Cécile Doubre², Ólafur Gudmundsson ⁴, Thibaut Barreyre ⁵, Sara Bazin¹ & Aurore Franco¹

Microearthquake hypocenters were analyzed in the Krýsuvík geothermal area in SW-Iceland with data taken from two consecutive passive seismic surveys, 2005 and 2009. Five years prior to the 2005 survey, this area was struck by an earthquake initiating a major top-to-bottom fluid migration in the upper crust. We observe from our surveys a complex bottom-to-top migration of seismicity with time following this fluid penetration, suggesting the migration of a pore pressure front controlled by the upper-crust fracture system. We interpret these data as the time and space development of high-temperature hydrothermal cells from a deep upper crustal fluid reservoir in the supercritical field. These results provide an insight into the coupling mechanisms between active tectonics and fluid flow in upper-crustal extensional systems with high thermal flux.

¹IUEM, CNRS, University of Western Brittany, Brest, France. ²EOST, CNRS, Université de Strasbourg, Strasbourg, France. ³Iceland GeoSurvey, Reykjavik, Iceland. ⁴Uppsala University, Uppsala, Sweden. ⁵Centre of Deep-Sea Research, University of Bergen, Bergen, Norway.
✉email: laurent.geoffroy@univ-brest.fr

Fluids in the crust are thought to play a crucial role in the release of both seismic and thermal energy, notably at divergent plate boundaries^{1,2}. However, the interplay between fluid circulation at the crustal scale and active fault tectonics remains poorly understood.

Fluids are expected to play a major role in the seismic cycle along large faults. Conceptual models such as the fault-valve model³ underline the role of variations in fluid pore pressure during the seismic cycle. Aseismic displacements along normal faults⁴ have also been explained by fluid-related processes, such as pressure solution creep⁵. Furthermore, abnormal low heat flow at spreading ridges outlines the importance of hydrothermal convection in the crust¹. At slow-spreading ridges, this convection is mainly located over heat sources (e.g. magma chambers, intrusions) at the middle of oceanic spreading segments^{6–11}. This hydrothermal convection is associated with seismic activity which differs from aftershock sequences^{2,12}. Earthquakes typically form clustered swarms of low-magnitude double-couple events^{13,14}. A key observation is that similar swarms are reproduced in fluid-injections in deep boreholes such as those related to hot dry rock (HDR) experiments¹⁵. Although it is not surprising that high fluid pressures favor shear activation within a fractured medium¹⁶, the cause of clustering of seismic activity within a large volume of the crust during short-duration sequences remains unclear. Processes of pore-pressure diffusion within a fractured rock mass are invoked¹⁷ triggered for instance by a distant or local seismic event¹⁸. Pore pressure diffusion is primarily controlled by fluid diffusivity, which itself depends on the permeability of the medium and fluid properties. At high temperatures, highly dynamic fluids can also propagate new cracks through stress corrosion¹⁹.

In hydrothermal systems of Iceland, fluids are mostly of seawater or/and meteoric origin, the hydrosphere being the feeding reservoir²⁰. Hydrothermal fluid flow within fractured media is illustrated by analytical and numerical modeling^{9,10,21}. However,

these models hardly account for the complexity of the circulation of a thermally driven fluid of unknown physical properties in a fractured medium whose permeability is probably anisotropic. A clear geophysical imaging through time of hydrothermal fluid circulation has not yet been presented. Although three-dimensional electrical resistivity tomography can image the structure of hydrothermal systems²², the temporal dimension is lacking, which is essential to elucidate the space–time pattern of hydrothermal fluid circulation.

Moreover, although the bulk bottom-to-top upwelling of hydrothermal fluids from heat sources (such as at the top of a magma chamber) is readily understood, the way fluids circulate top-to-bottom from the shallow crust to recharge the deeper crust is of major importance to our understanding of fluid flow in active volcano-tectonic settings. Crustal faults have been suggested to be a main contributor in this downward migration^{23–25}.

In this paper, we compare first-order results of two successive high-resolution seismic experiments in an active volcano-tectonic system with huge hydrothermal activity, the Krísuvík area, SW-Iceland^{26,27}.

We observe a remarkable upward migration of seismicity that we interpret as the development of convective hydrothermal fluid cells from the deep reservoir observed in the 2005 experiment²³. The fluids migrate through a highly permeable medium and reactivate pre-existing fault zones in the upper crust as conduits. The associated heat flux is estimated to be as high as that of large deep-sea hydrothermal systems. We show that the seismic cycle can control hydrothermal circulation in a divergent mafic system.

Geological and experimental settings

In Iceland, two overlapping spreading axes accommodate the divergent motion of the North American (NAM) and the Eurasian (EUR) plates (Fig. 1). These two axes are connected through the transform-like South Iceland Seismic Zone (SISZ). We focused our study on the Reykjanes peninsula (RP), a left-lateral shear-zone

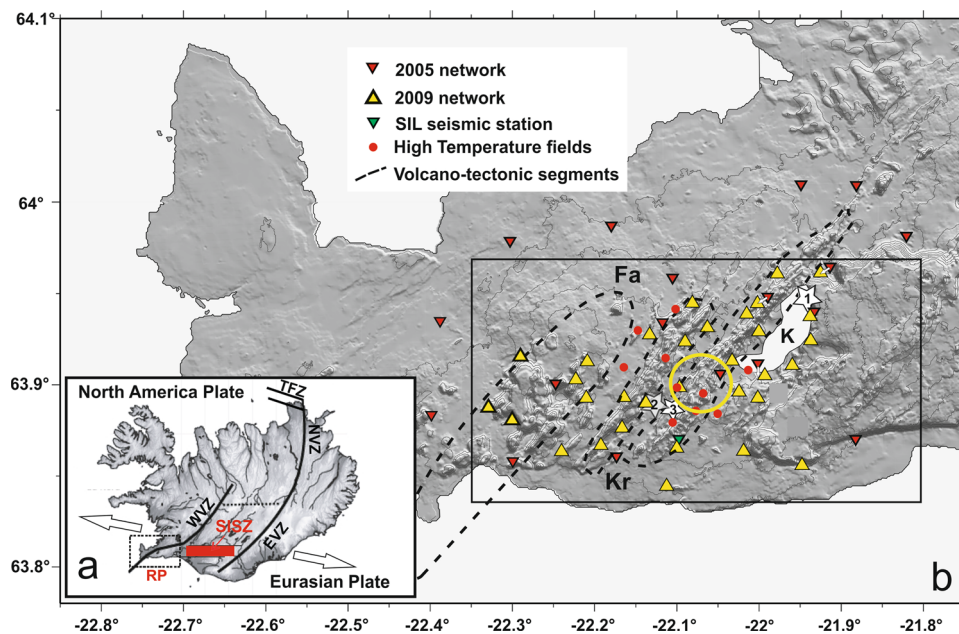


Fig. 1 Distribution of seismic stations during the Hydrorift experiments in the Reykjanes peninsula. **a** Tectonics of Iceland. Thick lines show main spreading axes. NVZ Northern Volcanic Zone, EVZ Eastern Volcanic Zone, WVZ Western Volcanic Zone, RP Reykjanes Peninsula, TFZ Tjörnes Fracture Zone, SISZ South Iceland Seismic Zone. Dashed rectangle locates the study area. **b** Map of the Hydrorift seismic networks on the Reykjanes peninsula. En-echelon SW-NE trending volcano-tectonic segments are delimited by dashed lines (Fa Fagradalsfjall, Kr Krísuvík); K Kleifarvatn. Stars show epicenters of three $M \geq 5$ strike-slip events²⁸: (1) Kleifarvatn earthquake, June 2000; (2) Núpshlíðarháls, June 2000; and (3) Mw 5.0, August 2003. Yellow circle shows the uplifted area measured by geodesy in the 2006–2008 period⁵¹. Digital elevation model was created from open data available from National Land Survey of Iceland.

connecting the Western Volcanic Zone to the Reykjanes oceanic ridge offshore^{23,27} (Fig. 1). The NAM–EUR plate boundary consists here of *en-echelon* volcano-tectonic segments or fissure swarms trending NE–SW that display intense hydrothermal activity in their central parts²⁷ (Fig. 1). In late 2020 and early 2021, the RP was highly active seismically and an unexpected volcanic eruption started March 2021 at Fagradalsfjall (Fig. 1).

Several $M_w \geq 5$ events (mostly strike-slip focal mechanisms) have occurred in the RP since 2000^{28,29} (Fig. 1). A $M_w > 5$ earthquake ruptured on June 17, 2000 a hidden NS-trending dextral fault bordering the eastern edge of lake Kleifarvatn^{30–32}. This rupture was part of a sequence of four $M_w > 5$ events dynamically triggered by the $M_w = 6.5$ SISZ Holt earthquake³¹. This event initiated a dramatic drop in the water level of Lake Kleifarvatn that lost up to 12% of its initial volume over a period of 16 months, due to local dilatancy of the fractured medium³². The main cracks trended N023–028E³², close to the dominant trend of the RP fracture system (Fig. 1), which is sub-perpendicular to the minimum principal stress, which is horizontal²⁸. This long-term lowering of the water table is distinct from transient (1–2 months) post-seismic pore flow in the shallow crust such as observed in the SISZ³³. Between April and September 2005, we conducted a passive seismological experiment around Krýsuvík and Fagradalsfjall on the Reykjanes Peninsula, SW Iceland, over a 5-month period²³ (Fig. 1). This early network allowed high precision of relocated earthquakes (estimated < 200 m both vertically and horizontally²³). The hypocenter distribution revealed a swarm-like seismicity distribution near Lake Kleifarvatn (Krýsuvík segment, Fig. 1). At this location, 75% of the hypocenters ranged from 4 to 5 km in depth and were located just above a low V_p/V_s ratio anomaly imaged by local-earthquake tomography (Fig. 2). This anomaly, which extended at least down to 6 km deep, was characterized by a 14% decrease of V_p/V_s ratio compared to the average estimated 1.78 for this area from wide-angle seismic refraction data³⁴. The anomaly was found to be due to low V_p only and probably related to compressible fluids in a fractured heat and fluid reservoir²³, most probably in supercritical conditions (i.e. $T > 374$ °C and $P_f > 22$ Mpa for pure water, $T > 426$ °C and $P_f > 29.8$ Mpa for seawater)³⁵. Since this deep reservoir was located beneath the area where the water table descended following the June 17, 2000 earthquake, it could have been fed from above due to a temporary increase of upper-crustal permeability associated with the strike-slip event²³. During the June 17, 2000 event, shear-induced dilatancy reactivated the conspicuous NNE–SSW to NE–SW trending fracture system^{30,32} and would have extended deep enough to create a connection between a shallow (0–2 km) hydrostatic fluid reservoir (i.e. with pore fluid pressure ratio $\lambda \sim 0.3$), associated with no micro-seismicity, and a deeper pressurized fluid reservoir^{23,36}. In accordance with this interpretation, fluids were trapped within the deeper heat reservoir after the closure of the system. This interpretation is certainly not unique but fluids chemistry from geothermal wells points to a superficial origin of fluids in the Iceland hydrothermal systems^{26,35}. To evaluate and strengthen this model both geometrically and dynamically, we conducted a second seismic experiment with a much denser network (Fig. 1). Our aim was to both refine the shape of the velocity anomaly and follow the spatial evolution of the fluid-driven microseismicity over a 4-year period.

Results

From May to October 2009, a new network with 32 seismic stations was operating over a 30 km² area across the Fagradalsfjall and Krýsuvík volcano-tectonic segments, with an average inter-station spacing of 3 km (Fig. 1). During the recording period,

more than 10,000 events were detected by our network in the central RP area. They mostly occurred during four intense episodic bursts, each lasting less than two days each (Fig. 2a). Each burst contained more than 1000 events.

Anomalous P-velocities with depth. The results yield better resolution than for the 2005 experiment, due to both the large number of events and the denser seismic network. In Fig. 2c, d, we report the V_p structure in terms of its 3D $V_p = 5 \text{ km s}^{-1}$ contour surface and along a vertical cross-section, respectively. An analysis of the detailed crustal V_p , V_s , and V_p/V_s structure in 3D is beyond the scope of this synthesis paper and will be detailed in a forthcoming contribution, including data from additional seismic networks. The V_p velocity model resulting from tomographic inversion of the 2009 dataset (Fig. 2c, d) improves upon the previous study conducted in 2005²³. Notably, we observed a deeper low- V_p anomaly at a depth down to 7 km with V_p variations exceeding 15% (Fig. 2d). There is an apparent continuity of the $V_p = 5 \text{ km s}^{-1}$ envelope from the deep up to the uppermost crust, following a curved area which extends eastward and upward beneath Lake Kleifarvatn (Fig. 2c). Note that the V_p/V_s ratio anomaly ($V_p/V_s = 1.65$ curve in Fig. 2c) shows a similar shape to the one evidenced with the 2005 dataset²³.

Seismicity distribution. Both the Krýsuvík and Fagradalsfjall areas display intense micro-seismic activity. We hereafter focused our data analysis and interpretation on the Krýsuvík–Kleifarvatn hydrothermal area. The epicenter distribution in the Krýsuvík segment showed that most of the activity is located to the SW of lake Kleifarvatn. This distribution mimics that of the active geothermal area (Fig. 1). Several short-duration clusters can be identified. Although the whole seismic cloud outlines a NE–SW-oriented distribution (like in 2005)²³, some shallow swarms ($\sim 2.5 \pm 1$ km in depth) appear to display a NS trend over short distances (~ 1.5 km; Figs. 2b and 3). The most obvious example is found at Nupshlidarhals (Figs. 2b and 3). At any depth, focal mechanisms within this swarm show a diversity of depth-independent movements ranging from purely extensional (dominant) to purely compressive types, with minor pure strike-slip mechanisms (Fig. 3).

Along the cross-section of Fig. 2d, we observe a clear dome-like shape of the deepest hypocenters defining the bottom of the seismogenic zone that mimics the convex edge of the top of the V_p/V_s anomaly. Above this curved surface we observe in Fig. 2d that the seismicity displays a remarkable 3D organization with several vertical peaks corresponding to the NS-trending clusters described in Figs. 2d and 3 in map-view section. A similar pattern with a dome-shaped seismicity as well as vertical and elongated seismic clusters has also been observed at the Katla volcano using a continuous 2.5-year passive seismic experiment³⁷.

Discussion

Several observations suggest that the recorded seismic bursts in the Krýsuvík geothermal area form swarms associated with high-fluid pressures in a fractured medium: (1) the short duration of the bursts (~ 2 days), (2) the low magnitude of the events, (3) the clustered space–time pattern^{38–40}. The variety of focal mechanisms at similar time and location (Fig. 3) precludes any tectonic interpretation for the seismic swarms. It is also noticeable that the decay rate of the seismicity in those seismic swarms does not follow the modified Omori–Utsu law⁴¹ even following the two largest in magnitude events (M_b : 4.5 and 4.4). This, and the permanent high-rate background micro-seismicity of the Krýsuvík–Kleifarvatn area, exclude aftershock interpretation for

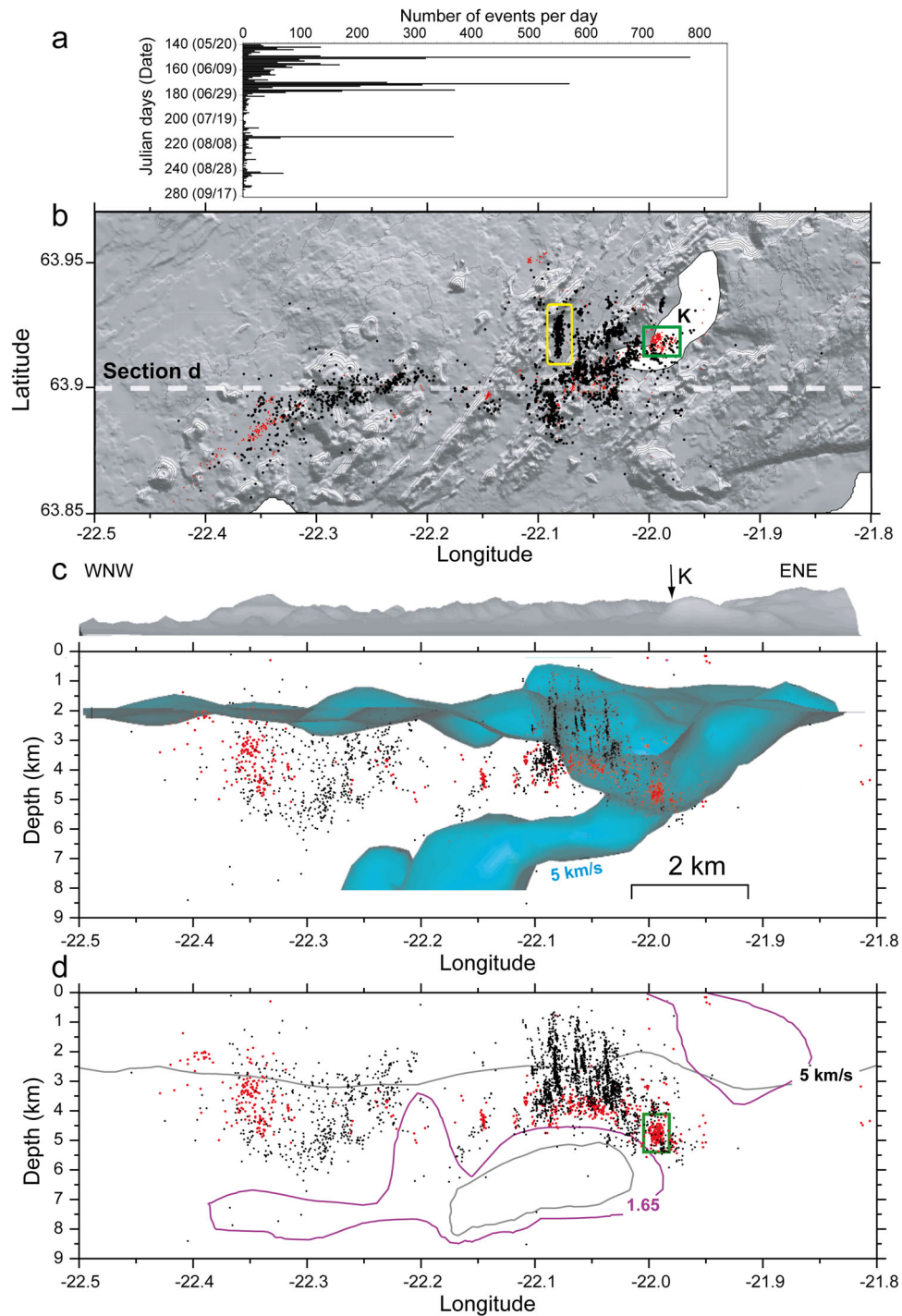


Fig. 2 Seismicity distribution during the 2005 and 2009 experiments. **a** Time distribution of the seismicity from the 2009 experiment. K: lake Kleifarvatn. The yellow rectangle is the location of the -NS-trending Nupshlidarhals swarm (see Fig. 3). **b** Map of the epicenters. Red and black dots are the events recorded during the 2005²³ and 2009 experiment, respectively. Green square indicates the location of the 2005 swarms used for permeability calculations (see Fig. 1 in Supplementary Material). The white dashed line shows the location of the cross section represented in (**d**); **c** 3D view of the low V_p anomaly ($V_p = 5$ km/s contour). **d** Hypocenters projected along an East-West cross-section (location in **a**). The black and purple lines represent the $V_p = 5$ km/s and $V_p/V_s = 1.65$ ratio contours, respectively.

the recorded seismicity and strongly supports a fluid-pressure interpretation within an overall dilatant tectonic area⁴².

Along the vertical cross-sections in Fig. 2c, d, we report results from both the 2005 and 2009 experiments. Most of the earthquakes in both data sets are shallower than 5.5 km. However, in the Krýsuvík-Kleifarvatn segment (Fig. 1), the 2005 events were located at the base of the seismogenic zone (between 3.8 and 5.5 km) while

the pattern drawn by 2009 hypocenters shows an upward vertical migration from the seismogenic basement towards the ground surface (i.e. from ~3.5 to ~1 km). Thus, we assume that the observed vertical migration of seismicity between 2005 and 2009 is related to an upward fluid flow (Fig. 4). This interpretation shares some similarity with that made further north in the Tjörnes Fracture Zone, albeit in a distinct tectonic context⁴³.

in the range of 10^{-13} – 10^{-14} m² is needed to numerically model hydrothermal fluid convection⁸. In addition, our $\sim 10^{-13}$ m² estimate is lower than the large value ($\sim 4 \times 10^{-11}$ m²) inferred for the fluid wave-like pulse propagation invoked to explain the Umbria–Marche seismic swarm⁵⁰. It is also lower than that inferred for the propagation of the 1989 Dobi extensional seismic swarms in Djibouti¹⁸.

Using the average value of 10^{-13} m² we estimated the associated heat flux mined at depth and transported advectively from the ‘reaction zone’ to be on the order of 500 kW m⁻¹ (see the ‘Methods’ section), a value comparable to what is extracted from large deep-sea hydrothermal systems^{9,11}.

Conclusion

The results described above give insights into hydrothermal fluid dynamics within active volcano-tectonic systems in Iceland. We suggest that the variation of the pattern of seismicity in the Krýsuvík–Kleifarvatn area over a 5-year period reflects a time-variation of fluid pressures within the upper crust. Increase of fluid pressures in a fractured reservoir may arise from a modification of the fracture geometry (size, shape, and density of fractures) and/or from an increase in volume of a compressible fluid within the fractures themselves^{16,17,36,42}. This increase in volume could arise from boiling and/or from input of new fluids within the fractured medium. Although we could not follow, step by step, the evolution of the pressure front with time, our two snapshots in 2005 and 2009 and the cell-like shape of the seismicity ‘pipes’ suggest that fluid escaped upward through a high-permeability medium, from the deep reservoir already imaged in 2005²³ (Fig. 4).

This upward migration of fluids in the studied area also corroborates geodetic observations. Both GPS and InSAR data showed evidence for local uplift at a rate of up to ~ 20 mm/yr between 2006 and mid-2009 southwest of Lake Kleifarvatn^{51,52} (Fig. 1) coeval with the unusually intense seismicity that we recorded during our 2009 experiment. We propose to correlate these geodetic data with the development of an increase in upper crustal pore pressure associated with the inferred bottom-to-top fluid diffusion. A positive correlation between uplift, seismicity and gas production (up to 100 T day⁻¹) is suspected in the Krýsuvík system⁵³.

These observations could complete the top-to-bottom model previously proposed²³. According to this model, in the standard state, the upper hydrostatic and generally aseismic shallow fluid reservoir is poorly connected to the deeper seismogenic lower reservoir where fluids are over pressurized and possibly, transiently, close to lithostatic conditions. Transition from the upper to the lower reservoir would be due to closure of downward cracks caused by the confining pressure and/or sealing of cracks by hydrothermal precipitates^{45,46}.

The lower reservoir would be recharged transiently by bulk increase of crustal dilatation associated with the deformation field around major faults during the co-seismic stage as this occurred following the Kleifarvatn event in 2000. In Kleifarvatn the communication between the two reservoirs associated with the transient increase of bulk crustal permeability lasted for ~ 16 – 18 months before closure of the system³².

The enhanced tomographic resolution from our 2009 experiment data shows that a low-Vp anomaly crosscuts the crust downward to the west (Figs. 2c and 4). This could indicate that a large fractured area with open cracks⁴², mostly trending NE–SW, extends from the ground surface (i.e. from the southern tip of Kleifarvatn) downward. We suggest in Fig. 4 that following the event in 2000 the upper-reservoir fluids percolated laterally and downward through this low-Vp fractured zone and were trapped within the deeper reservoir (explaining the 2005 seismicity). Most of the seismogenic fluids in 2005 were apparently located over the

low Vp-anomaly (located at depths over 5 km, see Fig. 2d). What is conveniently suggested by our data is that these fluids experienced a progressive increase in their enthalpy and ability to escape upward from the deep reservoir back to the hydrostatic one (Fig. 4). By combining geodetic and seismological observations it is suggested that a transient pore pressure front developed between 2005 and 2009 allowing the rapid establishment of a convective system (Fig. 4).

This proposed mechanism may indirectly, or directly, depends on regional tectonics. The larger-magnitude earthquakes on the Reykjanes Peninsula occur along sub-vertical NS-trending dextral faults^{29,54} that appear to have a role, albeit indirect, in the dynamics of fluid convection in the upper crust (this study). To the West of the Reykjanes Peninsula, those faults are localized in the volcanic/hydrothermal zones of Reykjanes, Fagradalsfjall and Krýsuvík^{29,54}. They are similar to those located further east in the EW-trending SISZ (Fig. 1a), which are best interpreted as consecutive to bookshelf faulting tectonics in relation to sinistral shear along a transform-like plate boundary²⁹. The plate boundary in the Reykjanes Peninsula is certainly more complex than in the SISZ^{23,29}. The Krýsuvík and Fagradalsfjall volcanic/hydrothermal centers could be located at the overstep of discrete \sim EW trending transform segments²³. Albeit still poorly constrained, this geometry could both promote transient periods of inter-seismic stress build-up and consecutive high fluid-pressures at depth⁴² followed by co-seismic sudden increase in crustal permeability.

Our observation of a possible recharge of a shallow reservoir from a deep reservoir in the inter-seismic period following a (partly silent?) earthquake appears of major interest in the understanding of the interrelationships between large-scale upper-crustal fluid flow and the seismic cycle. It offers a purely tectonic and mechanical explanation of the periodicity of the hydrothermal activity in hot extensional areas and builds on our understanding of fluid migrations in different tectonic settings^{25,55,56}.

Methods

Seismology. The Hydrorift 2009 network (Fig. 1) included 19 Geostar digitizers designed by EOST equipped with 3-component short-period sensors (Mark Products L22) recording continuously at a sampling rate of 125 Hz, and 13 Reftek digitizers from the National Icelandic pool, LOKI. Ten of those were equipped with 3-component Lennartz 5 s sensors and 3 with 3-component broad-band Geotech KS-2000M sensors recording continuously at a sampling rate of 100 Hz.

We manually picked the P and S-arrival times of 6100 events detected by at least 10 stations. The magnitude of the events remained below 2.0 for 98% of them, ranging from -0.5 to 4.5. First, the earthquakes were located using the local 1D Vp model^{34,57}. Second, arrival times for the 2830 best-located events, including differential arrival times measured by cross correlation, were inverted using TomoDD⁵⁸, which solves simultaneously absolute hypocenter locations with relative constraints and 3D P- and S-waves velocity structure. To increase the robustness of the velocity model as well as earthquake relocation, and to reduce dependency on the initial model velocity and the grid parametrization, we applied the post-processing weighted average model (WAM) method^{59,60}. This method consists of calculating a semblance-weighted average of many velocity models inverted with various geometries of the input velocity grid. It allows estimating the reliability of the velocity anomalies based on the standard deviation of the velocity values at each node of the fixed grid. The final uncertainty of hypocenter locations was estimated <140 m in the three directions.

Focal mechanism were determined using the FPFIT software⁶¹. We selected only events with minimum 10 picks and azimuthal gaps less than 135°.

Permeability estimates.

- From the whole hypocenter distribution

We estimated the mean flow velocity u from the distance Δz between the tops of the 2005 and 2009 seismogenic zones. We get a value of $\sim 2 \times 10^{-5}$ m s⁻¹.

The Darcy flow equation can be written as follow, with K the permeability:

$$K = (u \cdot \mu \cdot \Delta z) / \Delta P \quad (1)$$

μ is the mean fluid viscosity, and ΔP the fluid pressure drop along Δz .

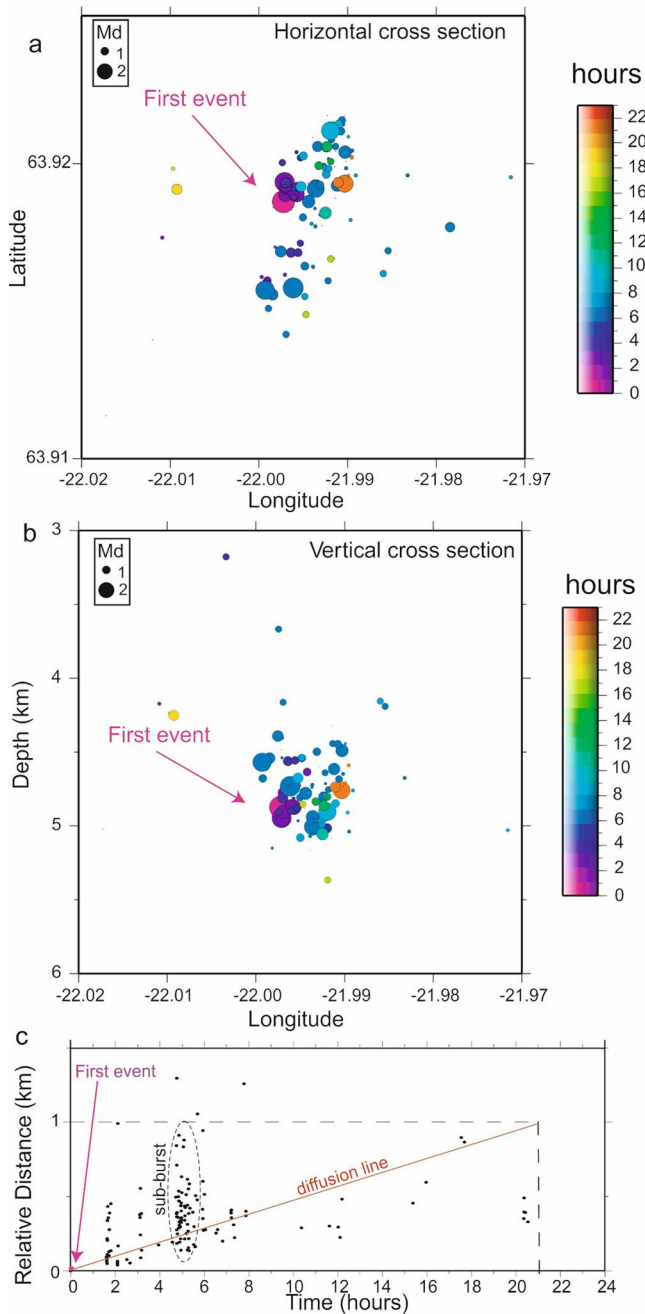


Fig. 5 Space-time evolution of hypocenters of a seismic swarm occurring on June 22, 2005, beneath Lake Kleifarvatn. **a** Map view, **b** EW vertical cross section, and **c** relative distance to the first event versus time.

We assume that fluids are over-pressured at any depth in the lower reservoir, i.e. the lambda factor (λ)⁶² is comprised between ~0.35 (hydrostatic pore pressure) and 1 (lithostatic pore pressure). According to this assumption, Eq. (1) can be rewritten as

$$K = (u \cdot \mu) / \lambda \cdot \rho_r \cdot g \tag{2}$$

with ρ_r , the averaged density of the upper crust. Using an average basalt density of $\rho_r = 2900 \text{ kg m}^{-3}$ ^{63,64} and an average viscosity of ~ 1 to $2 \times 10^{-4} \text{ Pa s}^{-1}$ for both the supercritical fluid and the overlying boiling water⁶⁵ we find from Eq. (2) an estimated permeability K comprised between $\sim 10^{-13}$ and $\sim 9 \times 10^{-13} \text{ m}^2$.

b. From pore-pressure diffusion in a seismic swarm.

We can also estimate the permeability in the Reykjanes crust from the volume of the independent seismic bursts themselves, taking into account a pore-pressure diffusion hypothesis (Fig. 5).

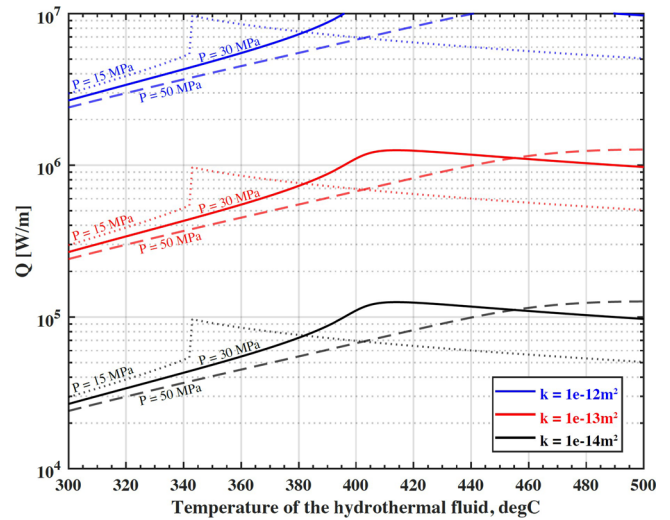


Fig. 6 Heat transported advectively by a hydrothermal fluid of temperature T_f for a given permeability k (line colors). Lines were computed from the Eq. (4) (i.e., Eq. (6) of Driesner⁶⁶), using a width for the hydrothermal plume (L_D) of 50 m and for fluid properties at 15, 30, and 50 Mpa shown as dotted lines, solid lines and dashed lines, respectively.

We chose one of the bursts from the 2005 experiment (location in Fig. 2c) with a sub-spherical external shape (i.e. closest to isotropic as possible) to estimate the “seismic” hydraulic diffusivity α_s from the migration of seismicity with time within a swarm ($\alpha_s = L^2 t^{-1}$)^{56,64}. Considering the distance between the initial seismic event and the final envelope of the following hypocenters we obtained a value of $12.6 \text{ m}^2 \text{ s}^{-1}$ for α_s (Fig. 5c). To infer the diffusivity we arbitrarily consider that the “instantaneous events” (or sub-bursts, Fig. 5c) at one time are equivalent to a single diffusion point which we locate at the closest distance from the first event. Those sub-bursts could tentatively be explained by very fast diffusion along pre-existing fractures. Doing that we obtain a lower value for α_s .

Permeability is related to fluid diffusivity through the equation⁶²:

$$K = (\mu \cdot \Phi \cdot \beta) \cdot \alpha \tag{3}$$

where Φ is the rock porosity, β the fluid compressibility, and α the hydraulic diffusivity. The seismic diffusivity α_s is within an order of magnitude of the true hydraulic diffusivity α ¹⁷. The average porosity in Iceland and comparable oceanic-type crust does not exceed 10% down to 2 km⁶³. The compressibility of supercritical fluids depends on temperature, pressure and composition of the fluid. It can be inferred from both analytical and experimental data⁶, that the compressibility of supercritical water at a depth of 4 km (lithostatic pressure of $\sim 120 \text{ MPa}$) and 400°C temperature, is about 10^{-9} Pa^{-1} with a 500 kg m^{-3} fluid density.

From Eq. (3), and at the depth of the chosen case example, we obtained values for K at an order of magnitude of $\sim 10^{-13} \text{ m}^2$ which is consistent with the value obtained in (a).

Heat flux estimates. We estimate the heat flux Q (W m^{-1}) that is transported advectively from the ‘reaction zone’ using the model developed by Driesner⁶⁶, which gives

$$Q \approx 2gk \cdot \left[\frac{\rho_f (h_f(T_f) - h_0) (\rho_0 - \rho_f(T_f))}{\mu_f(T_f)} \right] \cdot L \tag{4}$$

where g is the acceleration due to gravity (m s^{-2}), k is the permeability of the upflow zone (m^2), ρ is the density (kg m^{-3}) of the hydrothermal fluid (ρ_f) and of cold water (ρ_0), h is the specific enthalpy (J/kg) of the hydrothermal fluid (h_f) and cold water (h_0), T_f is the temperature of the hydrothermal fluid ($^\circ \text{C}$), μ_f is the dynamic viscosity of the hydrothermal fluid (Pa s), and L is the horizontal half-width of the hydrothermal plume (m). Note that Q is expressed in W m^{-1} which indicates heat flux per meter of volcano-tectonic segment length.

We assume a fluid saturated medium, under hydrostatic conditions, of homogenous isotropic permeability (k), which is varied from 10^{-12} to 10^{-14} m^2 in order to study the permeability effect on the evolving hydrothermal system. We describe average fluid properties in the system by taking fluid pressure at mid-height of the modeled hydrothermal system (i.e., simulations made for 15, 30, 50 Mpa) with temperatures varying from 300 to 500°C . The background cold fluid temperature is set to 4°C . We take into account the fluid density and specific enthalpy dependence with temperature and pressure. Finally, the half width of the hydrothermal plume is set to 50 m. Under these conditions and using the above equation, we estimate Q as a function of T_f and for different k (Fig. 6).

For an average permeability value of 10^{-13} m^2 , fluid properties taken at 30 Mpa (a reasonable average for the convective area that would be between 15 and 50 Mpa) and for fluid temperatures varying from 300 to 400 °C, we estimate heat flux values ranging from 3×10^5 to 10^6 W m^{-1} with an average of $5 \times 10^5 \text{ W m}^{-1}$ (for $T_f = 350 \text{ °C}$).

This average Q estimate of $\sim 500 \text{ kW m}^{-1}$ is of the same orders of magnitude than those of large deep-sea hydrothermal systems elsewhere^{11,67}.

Data availability

Files of the relocated hypocenters⁵⁷ from the 2005 and 2009 experiments (Figs. 2, 3, 4 and 5) and²³ are available at <https://doi.org/10.5061/dryad.6t1g1jx0w> with a readme.txt for use. Those data are part of ongoing research ending January 1, 2025.

Received: 23 June 2021; Accepted: 4 February 2022;

Published online: 10 March 2022

References

- Lister, C. R. B. On the thermal balance of a mid-ocean ridge. *Geophys. J. Res. Astron. Soc.* **26**, 515–535 (1972).
- Goslin, J. et al. Long-term seismicity of the Reykjanes Ridge (North Atlantic) recorded by a regional hydrophone array. *Geophys. J. Int.* **162**, 516–524 (2005).
- Sibson, R. H. Implications of fault-valve behavior for rupture nucleation and recurrence. *Tectonophysics* **211**, 283–293 (1992).
- Dobre, C. & Peltzer, G. Fluid-controlled faulting process in the Asal Rift, Djibouti, from 8-year radar interferometry observations. *Geology* **35**, 69–72 (2007).
- Gratier, J., Favreau, P. & Renard F. Modeling fluid transfer along California faults when integrating pressure solution crack sealing and compaction processes. *J. Geophys. Res.* **108**, <https://doi.org/10.1029/2001JB000380> (2003)
- Barclay, A. H., Toomey, D. R. & Solomon, S. C. Microearthquake characteristics and crustal Vp/Vs structure at the Mid-Atlantic Ridge, 35 N. *J. Geophys. Res.* **106**, 2017–2034 (2001).
- Lowell, R. P. & Germanovich, L. N. Hydrothermal processes at mid-ocean ridges: Results from scale analysis and single-pass models. In German, C.R., et al., eds., Mid-ocean ridges: hydrothermal interactions between the lithosphere and oceans. *AGU Geophys. Monogr.* **148**, 110–127 (2004).
- Coumou, D., Driesner, T., Geiger, S., Heinrich, C. A. & Matthäi, S. The dynamics of mid-ocean ridge hydrothermal systems: Splitting plumes and fluctuating vent temperatures. *E.P.S.L.* **245**, 218–231 (2006).
- Coumou, D., Driesner, T. & Heinrich, C. The structure and dynamics of mid-ocean ridge hydrothermal systems. *Science* **321**, 1825–1828 (2008).
- Fontaine, F., Cannat, M. & Escartin, J. Hydrothermal circulation at slow-spreading mid-ocean ridges: the role of along-axis variations in axial lithospheric thickness. *Geology* **36**, 759–762 (2008).
- Barreyre, T. et al. Structure, temporal evolution, and heat flux estimates from a deep-sea hydrothermal field derived from seafloor image mosaics. *Geochem. Geophys. Geosyst.* **13**, 1–29 (2012).
- Mochizuki, M., Brandsdóttir, B., Shiobara, H., Gudmundsson, G. & Stefansson, R. Detailed distribution of microearthquakes along the northern Reykjanes Ridge, off SW-Iceland. *Geophys. Res. Lett.* **27**, 1945–1948 (2000).
- Julian, B. R., Ross, A., Foulger, G. R. & Evans, J. R. Three-dimensional seismic image of a geothermal reservoir: The Geysers, California. *Geophys. Res. Lett.* **23**, 685–688 (1996).
- Fialko, Y. & Simmons, M. Deformation and seismicity in the Coso geothermal area, Inyo County, California: observations and modeling using satellite radar interferometry. *J. Geophys. Res.* **105**, 21781–21794 (2000).
- Charl y, J. et al. Large earthquakes during hydraulic stimulations at the geothermal site of Soultz-sous-For ts. *Int. J. Rock Mech. Min. Sci.* **44**, 1091–1105 (2007).
- Sibson, R. H. Structural permeability of fluid-driven fault-fracture meshes. *J. Struct. Geol.* **18**, 1031–1042 (1996).
- Talwani, P. & Acree, S. Pore pressure diffusion and the mechanism of reservoir-induced seismicity. *Pure Appl. Geophys.* **122**, 947–965 (1985).
- Noir, J. et al. Fluid flow triggered migration of events in the 1989 Dobi earthquake sequence of Central Afar. *Geophys. Res. Lett.* **24**, 2335–2338 (1997).
- Anderson, O. L. & Grew, P. C. Stress corrosion theory of crack propagation with applications to geophysics. *Rev. Geophys.* **15**, 77–104 (1977).
- Gregory, T. G. & Taylor, H. P. An oxygen isotope profile in a section of Cretaceous Oceanic Crust, Samail Ophiolite, Oman: evidence for ^{18}O buffering of the oceans by deep (>5 km) seawater-hydrothermal circulation at mid-ocean ridges. *J. Geophys. Res.* **86**, 2737–2755 (1981).
- Coumou D., Driesner, T., Geiger, S., Paluszny, A. & Heinrich C. A. High-resolution three-dimensional simulations of mid-ocean ridge hydrothermal systems. *J. Geophys. Res.* **114**, <https://doi.org/10.1029/2008JB006121> (2009)
- Revil, A. et al. Hydrogeology of Stromboli Volcano, Aeolian Islands (Italy) from the interpretation of resistivity tomograms, self-potential, soil temperature and soil CO₂ concentration measurements. *Geophys. J. Int.* **186**, 1078–1094 (2011).
- Geoffroy, L. & Dorbath, C. Deep downward fluid percolation driven by localized crust dilatation in Iceland. *Geophys. Res. Lett.* **35**, L17302 (2008).
- Cappa, F. Modelling fluid transfer and slip in a fault zone when integrating heterogeneous hydromechanical characteristics in its internal structure. *Geophys. J. Int.* **178**, 1357–1362 (2009).
- Dusunur, D. et al. Seismological constraints on the thermal structure along the Lucky Strike segment (Mid-Atlantic Ridge) and interaction of tectonic and magmatic processes around the magma chamber. *Mar. Geophys. Res.* **30**, 105–120 (2009).
- Arn rsson, S. Geothermal systems in Iceland: structure and conceptual models High-temperature areas. *Geothermics* **24**, 561–602 (1995).
- S mundsson, K., Sigurgeirsson, M.  . & Fri leifsson,  . Geology and structure of the Reykjanes volcanic system, Iceland. *J. Volcanol. Geotherm. Res.* **391**, 106501 (2020).
- Keiding, M., Arnad ttir, T., Sturkell, E., Geirsson, H. & Lund, B. Strain accumulation along an oblique plate boundary: the Reykjanes Peninsula, southwest Iceland. *Geophys. J. Int.* **172**, 861–872 (2008).
- Einarsson, P., Hjartard ttir,  . R., Hreinsd ttir S & Imsland, P. The structure of seismogenic strike-slip faults in the eastern part of the Reykjanes Peninsula Oblique Rift, SW Iceland. *J. Volcanol. Geotherm. Res.* **391**, <https://doi.org/10.1016/j.jvolgeores.2018.04.029> (2020)
- Pagli, C., Pedersen, R., Sigmundsson, F. & Feigl, K. L. Triggered fault slip on June 17, 2000 on the Reykjanes Peninsula, SW-Iceland captured by radar interferometry. *Geophys. Res. Lett.* **30**, 1273 (2003).
- Sudhaus, H. & J nsson, S. J. Improved source modelling through combined use of InSAR and GPS under consideration of correlated data errors: application to the June 2000 Kleifarvatn earthquake, Iceland. *Geophys. J. Int.* **176**, 389–404 (2009).
- Clifton, A., Pagli, C., J nsson, J. F., Eythorsd ttir, K. & Vogfj r, K. Surface effects of triggered fault slip on Reykjanes Peninsula, SW Iceland. *Tectonophysics* **369**, 145–154 (2003).
- J nsson, S., Segall, P., Pedersen, R. & Bj rnsson, G. Post-earthquake ground movements correlated to pore-pressure transients. *Nature* **424**, 179–183 (2003).
- Weir, N. et al. Crustal structure of the northern Reykjanes Ridge and Reykjanes Peninsula, southwest Iceland. *J. Geophys. Res.* **106**, 6347–6368 (2001).
- Fri leifsson, G.  . et al. 2020, The Iceland Deep Drilling Project at Reykjanes: drilling into the root zone of a black smoker analog. *J. Volcanol. Geotherm. Res.* **391**, <https://doi.org/10.1016/j.jvolgeores.2018.08.013>.
- Nur, A. & Walder, J. Hydraulic pulses in the Earth's crust. *Int. Geophys. Ser.* **51**, 461–473 (1992).
- Jeddi, Z., Tryggvason, A. & Gudmundsson,  . The Katla volcanic system imaged using local earthquakes recorded with a temporary seismic network. *J. Geophys. Res.* **121**, 7230–7251 (2016).
- Prejean, S., Stork, A., Ellsworth, W. Hill, D. & Julian B. (2003). High precision earthquake locations reveal seismogenic structure beneath Mammoth Mountain, California. *Geophys. Res. Lett.* **30**, 2247–2250 (2003)
- Hainzl, S. Seismicity patterns of earthquake swarms due to fluid intrusion and stress triggering. *Geophys. J. Int.* **159**, 1090–1096 (2004).
- Vidale, J. E. & Shearer, P. M. A survey of 71 earthquake bursts across southern California: exploring the role of pore fluid pressure fluctuations and aseismic slip as drivers. *J. Geophys. Res.* **111**, B05312 (2006).
- Utsu, T., Ogata, Y. & Matsu'ura, R. S. The centenary of the Omori formula for a decay law of aftershock activity. *J. Phys. Earth* **43**, 1–33 (1995).
- Miller, S. A. Aftershocks are fluid-driven and decay rates controlled by permeability dynamics. *Nat. Commun.* **11**, 5787 (2020).
- Hensch, M., Riedel, C., Reinhardt, J. & Dahm, T. Hypocenter migration of fluid-induced earthquake swarms in the Tj rnes Fracture Zone (North Iceland). *Tectonophysics* **447**, 80–94 (2008).
- Fortin, J., Stanchits, S., Vinciguerra, S. & Gu guen, Y. Influence of thermal and mechanical cracks on permeability and elastic wave velocities in a basalt from Mt. Etna volcano subjected to elevated pressure. *Tectonophysics* **503**, 60–74 (2011).
- Bergerat, F., Saemundsson, K., Fourel, L. & Angelier, J. Structure and activity of the geothermal field of Hvalfj r ur (Iceland) from brittle tectonic, geothermal and paleostress analysis. *Bull. Soc. G ol. Fr.* **184**, 451–465 (2013).
- Liotta, D. et al. Fracture analysis, hydrothermal mineralization and fluid pathways in the Neogene Geitafell central volcano: insights for the Krafla active geothermal system, Iceland. *J. Volcanol. Geotherm. Res.* **391**, <https://doi.org/10.1016/j.jvolgeores.2018.11.023> (2020)

47. Byerlee, J. Friction, overpressure and fault normal compression. *Geophys. Res. Lett.* **17**, 2109–2112 (1990).
48. Adelinet, M., Dorbath, C., Le Ravalec, M., Fortin, J. & Guéguen, Y. Deriving microstructure and fluid state within the Icelandic crust from the inversion of tomography data. *Geophys. Res. Lett.* **38**, L03305 (2010).
49. Becker, K. Measurements of the permeability of the sheeted dikes in Hole 504B, ODP Leg 111. *Proc. Ocean Drill. Program Sci. Results* **111**, 317–325 (1989).
50. Miller, S. A. et al. Aftershocks driven by a high-pressure CO₂ at depth. *Nature* **427**, 724–727 (2004).
51. Keiding, M., Árnadóttir, T., Jónsson, S. J., Decriem & Hoop, A. Plate boundary deformation and man-made subsidence around geothermal fields on the Reykjanes Peninsula, Iceland. *J. Volcanol. Geotherm. Res.* **194**, 139–149 (2010).
52. Michalczywska, K. et al. The inflation and deflation episodes in the Krýsuvík geothermal area. In *American Geophysical Union, Fall Meeting*, V53A-V52589 (AGU, San Francisco, CA, 2011).
53. Gudjónsdóttir, S. R. et al. Gas emissions and crustal deformation from the Krýsuvík high temperature geothermal system, Iceland. *J. Volcanol. Geotherm. Res.* **391** <https://doi.org/10.1016/j.jvolgeores.2018.04.007> (2020).
54. Keiding, M., Lund, B. & Árnadóttir, T. Earthquakes, stress and strain along an obliquely divergent plate boundary: the Reykjanes Peninsula, southwest Iceland. *J. Geophys. Res.* **114**, B09306 (2009).
55. Chiarabba, C., De Gori, P. & Boschi, E. Pore-pressure migration along a normal-fault system resolved by time-repeated seismic tomography. *Geology* **37**, 67–70 (2009).
56. Nascimento, A. F., Cowie, P. A., Lunn, R. J. & Pearce, R. G. Spatio-temporal evolution of induced seismicity at Açú reservoir, NE Brazil. *Geophys. J. Int.* **158**, 1041–1052 (2004).
57. Waldhauser, F. *HypoDD: A Computer Program to Compute Double-difference Earthquake Locations*. USGS Open File Report, 01-113 (USGS, 2001)
58. Zhang, H. & Thurber, C. Double-difference tomography: the method and its application to the Hayward Fault, California. *Bull. Seismol. Soc. Am.* **93**, 1875–1889 (2003).
59. Calò, M., Dorbath, C., Luzio D., Rotolo, S. & Danna G. Local earthquakes tomography in the southern Tyrrhenian region of Italy: Geophysical and petrological inferences on the subducting lithosphere. In *Subduction Zone Geodynamics. Front. Earth Sci.* 85–89. (eds Lallemand, S. & Funicello, F.) (Springer, Berlin, Heidelberg, 2009).
60. Calò, M., Dorbath, C., Cuenot, N. & Cornet, F. Large scale aseismic motion identified through 4D P wave tomography. *Geophys. J. Int.* **186**, 1295–1314 (2011).
61. Reasenber, P. & Oppenheimer, D. *FPPIT, FPLOT and FPPAGE: Fortran Computer Programs for Calculating and Displaying Earthquake Fault-plane Solutions*. USGS Open-File Report 85-739 (USGS, 1985) <https://doi.org/10.3133/ofr85739>.
62. Sibson, R. H. Earthquake rupturing in fluid-pressured crust: how common? *Pure Appl. Geophys.* **171**, 2867–2885 (2004).
63. Jónsson, G. & Stefánsson, V. Density and porosity logging in the IRDP Hole, Iceland. *J. Geophys. Res.* **87**, 6619–6630 (1982).
64. Franzson, H. Reservoir geology of the Nesjavellir high-temperature field in SW-Iceland. In *Proceedings of the 19th Annual PNOC-EDC Geothermal Conference*, Manila, Philippines, 13–20 (PNOC Energy Development Corporation, 1998).
65. Kalinichev, A. G. Molecular simulations of liquid and supercritical water: Thermodynamics, structure, and hydrogen bonding. *Rev. Mineral. Geochem.* **42**, 83–129 (2001).
66. Driesner, T. The interplay of permeability and fluid properties as a first order control of heat transport, venting temperatures and venting salinities at mid-ocean ridge hydrothermal systems. *Geofluids* **10**, 132–141 (2010).
67. Lowell, R. P., Farough, A., Hoover, J. & Cummings, K. Characteristics of magma-driven hydrothermal systems at oceanic spreading centers. *Geochem. Geophys. Geosyst.* **14**, 1756–1770 (2013).

Acknowledgements

The Hydrorift experiment was part of the Geoflux program supported by the Pays de La Loire Region. We thank Nabil Sultan (IFREMER, France) for his comments about permeability estimates and Thorbjorg Agustsdottir (ISOR, Iceland) for her help in seismic data processing. We warmly thank the three reviewers for their constructive comments, which improved the overall quality of this work.

Author contributions

L.G. wrote down the paper. He was principal investigator of the scientific program, co-designed the experiments and set down the conceptual model. C.Dor. co-designed the 2005 and 2009 experiments and supervised seismic data treatment including tomography. K.Á. co-designed the 2009 experiment, carried out data collection and data treatment and supervised part of the interpretation of the data. S.K. performed part of 2009 data treatment and analysis, notably focal mechanisms. Ó.G.F. co-led the 2009 seismic survey in Iceland and added expertise on geothermal processes in Iceland. C.Dou. co-supervised part of the seismic data processing and manuscript editing. Ó.G. appraised the seismic analysis and manuscript editing. T.B. performed heat flux computation and wrote down the related text in the Methods section. S.B. helped in data analysis and text editing. A.F. performed the seismic processing from the 2009 raw data.

Competing interests

The authors declare no competing interests.

Additional information

Supplementary information The online version contains supplementary material available at <https://doi.org/10.1038/s43247-022-00382-0>.

Correspondence and requests for materials should be addressed to Laurent Geoffroy.

Peer review information *Communications Earth & Environment* thanks Stephen A. Miller, Wilfred A. Elders and the other, anonymous, reviewer for their contribution to the peer review of this work. Primary Handling Editors: Luca Dal Zilio, Joe Aslin.

Reprints and permission information is available at <http://www.nature.com/reprints>

Publisher's note Springer Nature remains neutral with regard to jurisdictional claims in published maps and institutional affiliations.

 **Open Access** This article is licensed under a Creative Commons Attribution 4.0 International License, which permits use, sharing, adaptation, distribution and reproduction in any medium or format, as long as you give appropriate credit to the original author(s) and the source, provide a link to the Creative Commons license, and indicate if changes were made. The images or other third party material in this article are included in the article's Creative Commons license, unless indicated otherwise in a credit line to the material. If material is not included in the article's Creative Commons license and your intended use is not permitted by statutory regulation or exceeds the permitted use, you will need to obtain permission directly from the copyright holder. To view a copy of this license, visit <http://creativecommons.org/licenses/by/4.0/>.

© The Author(s) 2022, corrected publication 2022